JOURNAL OF GEOPHYSICAL RESEARCH, VOL. 114, C07010, doi:10.1029/2008JC005031, 2009

Stabilizing effect of random waves on rip currents

Haider Hasan,[1,2] Nicholas Dodd,[1] and Roland Garnier[1,3]

Received 18 July 2008; revised 16 February 2009; accepted 16 April 2009; published 9 July 2009.

[1] The instability leading to the formation of rip currents in the nearshore for normal waves on a nonbarred, nonerodible beach is examined with a comprehensive linear stability numerical model. In contrast to previous studies, the hypothesis of regular waves has been relaxed. The results obtained here point to the existence of a purely hydrodynamical positive feedback mechanism that can drive rip cells, which is consistent with previous studies. This mechanism is physically interpreted and is due to refraction and shoaling. However, this mechanism does not exist when the surf zone is not saturated because negative feedback provided by increased (decreased) breaking for positive (negative) wave energy perturbations overwhelms the shoaling/refraction mechanism. Moreover, turbulent Reynolds stress and bottom friction also cause damping of the rip current growth. All the nonregular wave dissipations examined give rise to these hydrodynamical instabilities when feedback onto dissipation is neglected. When this feedback is included, the dominant effect that destroys these hydrodynamical instabilities is the feedback of the wave energy onto the dissipation. It turns out that this effect is strong and does not allow hydrodynamical instabilities on a planar beach to grow for random seas.

Citation: Hasan, H., N. Dodd, and R. Garnier (2009), Stabilizing effect of random waves on rip currents, *J. Geophys. Res.*, *114*, C07010, doi:10.1029/2008JC005031.

1. Introduction

[2] Normally incident waves approaching a straight shoreline shoal and eventually break. This generates set-up (increased elevation in mean free surface), through radiation stresses [*Longuet-Higgins and Stewart*, 1962, 1964], and therefore also offshore directed horizontal pressure gradients. In theory this dynamical balance can pertain along an alongshore uniform shore with correspondingly uniform wave conditions. In reality water is often seen to recirculate back to sea at certain locations, in rip currents, which are, in turn, fed by alongshore flowing currents on either side.

[3] Studies have shown that rip currents may approach speeds of up to 2 m s^{-1} [see *MacMahan et al.*, 2006], although the average strength is often less than that. These circulations therefore can become an issue for beach safety [see *Short and Hogan*, 1994]. Nearshore circulation also results in the circulation of cleaner water from the offshore into the nearshore region [see *Inman et al.*, 1971]. Importantly, nearshore circulation together with waves also transport beach sediment, and indeed the rips themselves apparently erode rip channels. Hence it is vital to understand the physical mechanisms of the generation of rip currents if we are to understand the nearshore sediment budget. It should be noted, however, that it is not clear whether these channels are passively eroded by the currents, or if the channels appear in combination with the currents as part of a dynamical interaction. We return to this point later.

[4] On a long straight coast, rip currents can occur at quite regular intervals so one can often assign an alongshore spacing to these features, which ranges from 50 to 1000 m [*Short*, 1999], and as reported by *Short* [1999], rip currents are most readily formed on intermediate energetic beaches characterized by slopes of 1:30 to 1:10. This quasi-regularity in spacing of rip currents is intriguing, and has received some attention in previous studies.

[5] Early observational studies of rip currents in the field such as that made by *Shepard et al.* [1941] and *Shepard and Inman* [1950], and more recent ones by *Brander and Short* [2000] and *MacMahan et al.* [2005], have found rip currents to occur where there are alongshore variations in the bathymetry with rip channels cut through the alongshore bar. This alongshore variation in the bathymetry results in an accompanying variation in wave height. These wave height variations generate alongshore variable pressure gradients that drive nearshore circulation cells. Experimental studies in laboratories have also supported this idea where measurements were conducted for a barred beach profile with incised rip channels [see *Haller et al.*, 2002; *Haas and Svendsen*, 2002]. Using the concept of radiation stresses, *Bowen* [1969] showed that nearshore circulation cells, including rips, can be forced by imposing alongshore variations in wave height on a plane sloping beach for waves normal to the shoreline. The alongshore variation in wave height results in corresponding

[1]Environmental Fluid Mechanics Research Centre, Process and Environmental Division, Faculty of Engineering, University of Nottingham, Nottingham, UK.

[2]Now at Department of Mathematics and Basic Sciences, NED University of Engineering and Technology, Karachi, Pakistan.

[3]Now at Applied Physics Department, Universitat Politecnica de Catalunya, Barcelona, Spain.

0148-0227/09/2008JC005031$09.00

variations in radiation stresses, thus driving the circulation cells as areas of large set-up (large wave height) drive a current alongshore into the rips.

[6] The model of *Bowen* [1969], however, does not explain the quasiperiodicity itself, and nor does it consider an erodible beach. Attention has therefore subsequently been focused on examining the stability to periodic perturbations of alongshore uniform setup on an erodible beach, namely, the morphodynamical stability. The pioneering study of *Hino* [1974] identified such an instability, and, for normal incident waves, rip currents/channels were formed together with cuspate morphological features when an alongshore periodic perturbation was imposed. This theory was substantially progressed by *Deigaard et al.* [1999] and an instability mechanism identified by *Falqués et al.* [2000], who noted that the potential stirring (depth-averaged concentration) gradient governed the positive feedback mechanism by which the rips and their associated morphology evolve. Thus, for an offshore flowing current (the rip), any negative perturbation (the incipient rip channel) will be enhanced (positive feedback, and therefore instability) where the concentration is increasing offshore, because the current flows from regions of lower to greater concentration, so that erosion must take place for the concentration profile to be maintained. Studies with more comprehensive models have been presented by *Damgaard et al.* [2002], *Caballeria et al.* [2002], *Calvete et al.* [2005], and *Garnier et al.* [2006].

[7] These explanations have focused on morphodynamical instability. However, it has also been suggested that alongshore variations in wave height may arise as a result of wave - current interaction, which poses the question about the formation of rip channels alluded to earlier: do channels and currents form together as a morphodynamical instability, or do rip currents form as a hydrodynamical instability and then erode the channels. The episodic nature of rip currents observed by *Smith and Largier* [1995] at Scripps beach possibly indicates that rip currents are a result of a hydrodynamic instability, but these events could also be due to temporal variations in the incoming wavefield [*Reniers et al.*, 2004]. Field evidence of rip currents without channels is hard to find. *MacMahan et al.* [2006] note that all currents are accompanied by perturbations in the bed level, albeit small ones at some locations. The laboratory investigation by *Bowen and Inman* [1969] on a plane sloping beach found rip currents generated as a result of the interaction between edge waves and incoming incident waves, with rip spacing equal to (and therefore dictated by) the alongshore wavelength of the edge wave. Nevertheless, some other studies have continued to consider the purely hydrodynamical instability (or something akin to this) to investigate whether rip currents can be formed without perturbations in the bed.

[8] The analytical study of *Dalrymple and Lozano* [1978], who extended the work of *LeBlond and Tang* [1974], suggested that wave refraction and shoaling (as opposed to shoaling alone) was responsible for the existence of rip currents. The authors considered normally incident waves on a planar foreshore of constant slope and a flat offshore bathymetry, on which they imposed an alongshore periodic perturbation (neither growing nor decaying), and noted that the interaction of the wavefield with the offshore currents acts to intensify them.

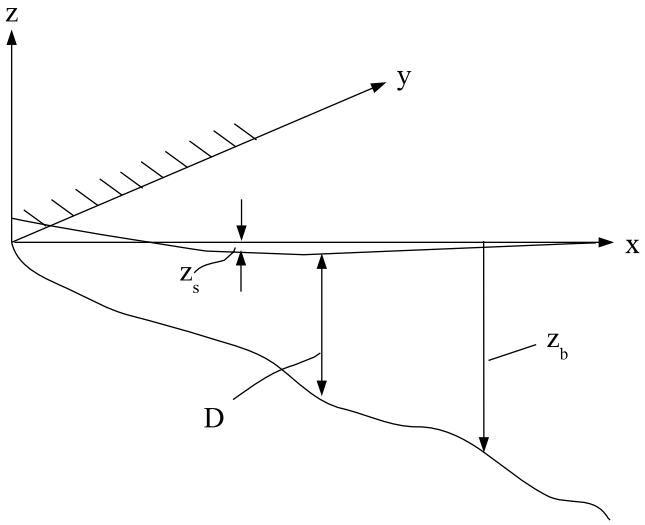

Figure 1. Sketch of the nearshore coordinate system and the general bathymetry.

[9] For incoming waves normal to the shoreline, *Falqués et al.* [1999] examined the growth of nearshore circulation cells (rip cells) using linear stability analysis (thus allowing growing modes) on a non-erodible, plane beach. Two cases were considered. The first was set-up in isolation; that is, waves were normally incident on a monotonic beach and wave refraction because of current neglected. An analytical analysis showed that the set-up did not induce instability. The subsequent inclusion of wave refraction on current, the second case, led to instability. Here *Falqués et al.* [1999] considered a simplistic situation in which waves approached over a flat bathymetry, and perturbations in wave energy dissipation due to wave breaking were neglected. The flat bed was chosen so as to avoid dealing with wave breaking and the discontinuities at the breaking line, and to allow the application of shallow water theory throughout.

[10] An alternative hydrodynamical rip current study was made by *Murray and Reydellet* [2001]. The focus of their study was on self-organized rip currents driven by a feedback involving a newly hypothesized interaction between waves and currents, in which the rip current causes a diminution in wave height, through turbulence generated by shears in orbital velocities. This would then lead to reduced shoreline set-up, now no longer balanced because of decrease in wave height, which then leads to alongshore flows into the rip. A simple model with effects of currents on wave number field not included was developed on the basis of cellular automata where each variable defined in a particular cell in a grid of cells interacted according to rules encapsulating the above physics, which then indeed led to a positive feedback that intensified the current [see *Murray and Reydellet*, 2001].

[11] *Yu* [2006] examined the growth of rip current cells due to the inclusion of wave-current interactions. This was motivated by the uncertainties in the results obtained by *Dalrymple and Lozano* [1978].

[12] Assuming monochromatic waves, *Yu* [2006] split the cross-shore domain into an offshore part (prior to breaking)

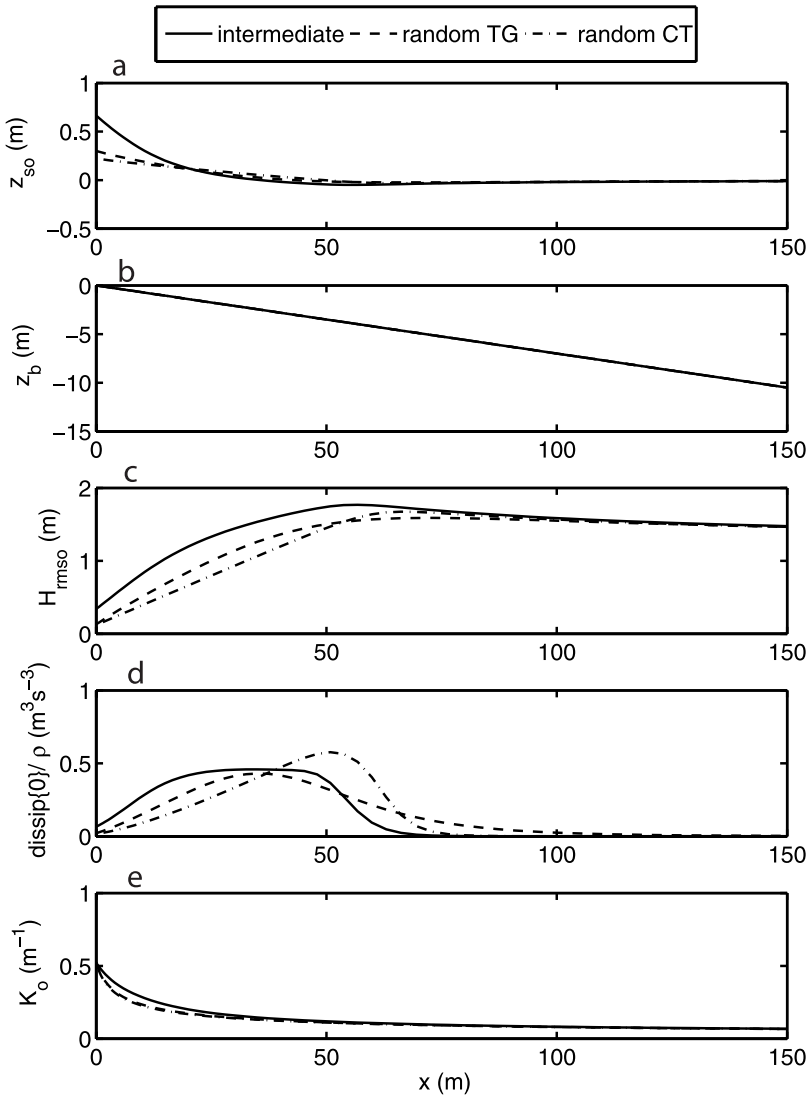

Figure 2. Basic state cross-shore profiles for different types of waves, i.e., intermediate and random (both *Thornton and Guza* [1983] (TG) and *Church and Thornton* [1993] (CT)) on a plane sloping beach profile with beach slope $\beta = 0.07$, $H_{rmso\infty} = 1.5$ m, and $T = 10$ s: (a) mean surface elevation, (b) bed level, (c) root mean square wave height, (d) wave energy dissipation, and (e) wave number.

mostly on constant depth and therefore allowing shallow water theory to be used in the offshore portion of the domain, and a part in the surf zone (plane beach). Before breaking a wave energy equation is implemented to transform wave height; within the surf zone the wave height is controlled by the local water depth. The break point occurs on the slope, and a moving shoreline is implemented.

[13] For an offshore wave height H_∞ of 1.88 m and period $T = 8.17$ s *Yu* [2006] predicts a growing "rip cell" mode with *e*-folding time 14.83 s. This increased rapidly for smaller wave heights: $H_\infty = 1.12$ m possessed an *e*-folding time of 97.20 s. The comparison of predicted rip-spacing with field observations showed fairly good agreement for large wave breaker heights. However, for smaller breaker heights the agreement was poor. For more details, see *Yu* [2006].

[14] The idealized nature of the study of *Falqués et al.* [1999] and the more sophisticated but still restricted (e.g., shallow water theory and the use of regular waves) study of *Yu* [2006], thus leads us to re-examine the hydrodynamical instability to alongshore periodic disturbances of normally incident waves on a plane beach, but this time using a comprehensive model incorporating finite depth wave propagation and random waves. To this end we investigate the possible formation of rip cells under more realistic conditions (random waves) using the model of *Calvete et al.* [2005], which also includes other effects (e.g., turbulent Reynolds stresses) not considered by the earlier authors.

[15] In section 2, we describe the model used in the present study. In section 3, we show results for the numerical investigations. Thereafter we draw some conclusions.

2. Model Description

[16] The model used here is described in detail by *Calvete et al.* [2005]. It is based on the depth and time averaged mass (1) and momentum (2) equations and wave energy (3),

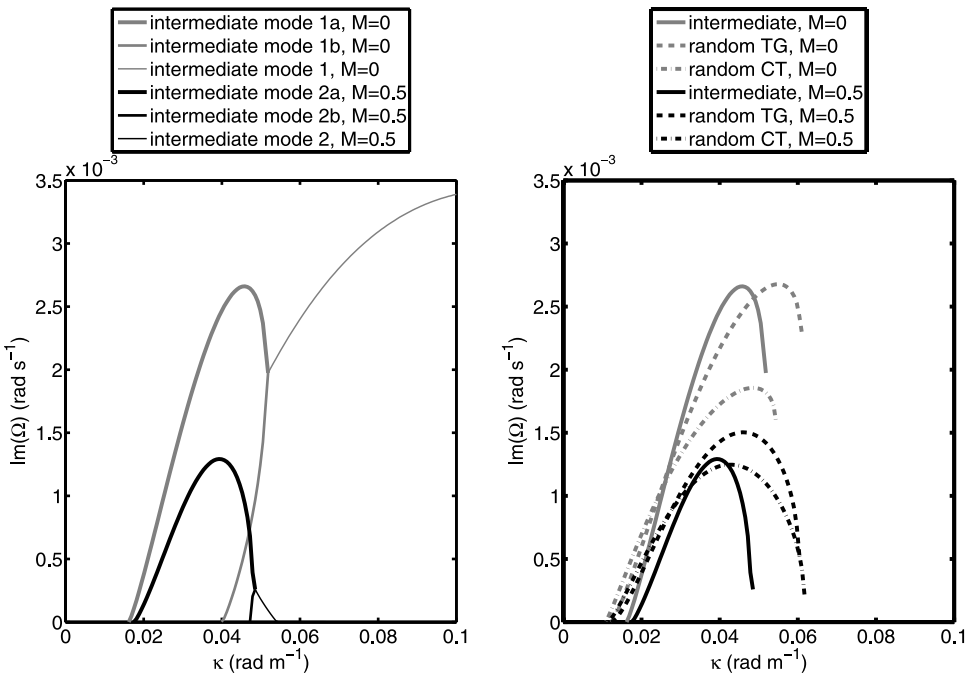

Figure 3. Rip current growth rate curves for different wave types, i.e., intermediate and random (both *Thornton and Guza* [1983] (TG) and *Church and Thornton* [1993] (CT) cases) with no feedback of perturbations on $\mathcal{D}$ for $H_{rmso\infty} = 1.5$ m, $T = 10$ s, $\beta = 0.07$, and $z_o = 0.001$ m and when Reynolds Stress terms are turned on and off, i.e., $M = 0$ and $M = 0.5$.

wave phase (4), and sediment conservation equations. Since we are examining hydrodynamical instabilities we do not consider the sediment conservation equation here. The governing equations are

$$\frac{\partial D}{\partial t} + \frac{\partial D v_i}{\partial x_i} = 0, \tag{1}$$

$$\frac{\partial v_i}{\partial t} + v_j \frac{\partial v_i}{\partial x_j} = -g\frac{\partial z_s}{\partial x_i} - \frac{1}{\rho D}\frac{\partial}{\partial x_j}\left(S'_{ij} - S''_{ij}\right) - \frac{\tau_{bi}}{\rho D}, \tag{2}$$

$$\frac{\partial E}{\partial t} + \frac{\partial}{\partial x_i}\left(\left(v_i + c_{gi}\right)E\right) + S'_{ij}\frac{\partial v_j}{\partial x_i} = -\mathcal{D}, \tag{3}$$

$$\frac{\partial \Phi}{\partial t} + \sigma + v_i \frac{\partial \Phi}{\partial x_i} = 0, \tag{4}$$

where $i, j = 1, 2$, so $x_i = (x_1, x_2) = (x, y)$, where x and y are cross-shore and alongshore coordinates. Horizontal velocities are $v_i = (v_1, v_2) = (u, v)$, g is acceleration due to gravity and ρ is water density. Total water depth is denoted $D = z_s - z_b$, where z_s is the mean surface elevation and z_b is the (fixed) bed level: see Figure 1. Further, $E = \frac{1}{8}\rho g H_{rms}^2$ is wave energy density, where H_{rms} is root mean squared wave height, Φ is the wave phase, S'_{ij} are the components of the radiation stress tensor, S''_{ij} are the Reynolds stress tensor components, τ_{bi} is the ith component of the bottom friction, $\mathcal{D}$ is the dissipation due to wave breaking, and c_{gi} are the group velocity vector components. σ is the intrinsic frequency given by

$$\sigma = \sqrt{gK\tanh(KD)}, \tag{5}$$

where K is the wave number ($K = |\vec{K}|$). The wave vector $\vec{K}$ is given by $\vec{K} = \vec{\nabla}\Phi$.

[17] The expression for the Reynolds' stresses applied here is [see, e.g., *Svendsen*, 2006]

$$S''_{ij} = \rho\nu_t D\left(\frac{\partial v_i}{\partial x_j} + \frac{\partial v_j}{\partial x_i}\right), \tag{6}$$

where the *Battjes* [1975] parameterization for horizontal eddy viscosity has been implemented

$$\nu_t = M\left(\frac{\mathcal{D}}{\rho}\right)^{\frac{1}{3}} H_{rms}, \tag{7}$$

where M is a parameter that characterizes turbulence and is of $O(1)$. *Calvete et al.* [2005] choose $M = 1$ [*Battjes*, 1975]. However, *Svendsen et al.* [2002] recommended $0.05 < M < 0.1$. Here we take a default value $M = 0.5$. Bed shear stress is parameterized using a linear friction law:

$$\tau_{bi} = \rho\left(\frac{2}{\pi}\right) C_D u_{rms} v_i, \tag{8}$$

where C_D is the drag coefficient and is given as

$$C_D = \left(\frac{0.40}{\ln(D/z_o) - 1}\right)^2, \tag{9}$$

where z_o is the bed roughness length (default value taken as z_o = 0.001 m), and u_{rms}, wave orbital velocity at the substitute for the boundary layer edge, is determined using linear theory:

$$u_{rms} = \frac{H_{rms}}{2}\frac{gK}{\sigma}\frac{\cosh Kz_o}{\cosh KD}. \tag{10}$$

2.1. Wave Energy Dissipation

[18] In real seas waves are random and so will not break at one point. As a result, the surf zone can be quite extensive compared to that for quasi-regular waves. For random waves, breaking can be a result of short wave interaction, the interaction of waves with the bottom, current or wind [*Roelvink*, 1993]. Here the interaction of current and wind are neglected, and wave transformation is linear. Therefore, wave breaking is dictated by the effect of changes in the seabed (for energy dissipation due to current-limited wave breaking, see *Chawla and Kirby* [2002]). Apart from these simplifications, which were also imposed by *Yu* [2006] and *Falqués et al.* [1999], the effects of different types of random wave breaking are here examined in detail. This is motivated both by the consideration of regular waves in previous studies, and by related work [see *Van Leeuwen et al.*, 2006] that showed the importance of the type of wave breaking on the evolution of bed forms.

[19] Three types of random waves are considered here. They are distinguished by the extent of the surf zone and the size and shape of the dissipation profile, and are implemented by changing the energy dissipation term $\mathcal{D}$ in (3), so that they describe transition between random and quasi-regular (intermediate) waves. We use the models of *Thornton and Guza* [1983] and *Church and Thornton* [1993], the first because it is standard in the literature and the second because it allows for somewhat more concentrated breaking at the shore. The model of *Church and Thornton* [1993] is

$$\mathcal{D} = \frac{3\sqrt{\pi}}{16}\rho g B^3 f_p \frac{H_{rms}^3}{D}\left\{1 + \tanh\left[8\left(\frac{H_{rms}}{\gamma_b D} - 1\right)\right]\right\} \times \left[1 - \left(1 + \left(\frac{H_{rms}}{\gamma_b D}\right)^2\right)^{-5/2}\right], \tag{11}$$

where B = 1.3 (describes the type of breaking) and γ_b = 0.42 are used, and where $f_p = \sigma/2\pi$ is the intrinsic peak frequency (for *Thornton and Guza* [1983], B = 1 and γ_b = 0.42).

[20] The model of *Van Leeuwen et al.* [2006], which is based on that of *Roelvink* [1993], and which allows for regular, depth-limited regular and random waves, is used here for what we term "intermediate" waves, to provide the link between regular and fully random waves. This thus allows us to suggest trends as we move toward regular waves, the situation examined by earlier authors. For intermediate waves B = 1 and γ_b = 0.55. See Appendix A for these dissipation expressions.

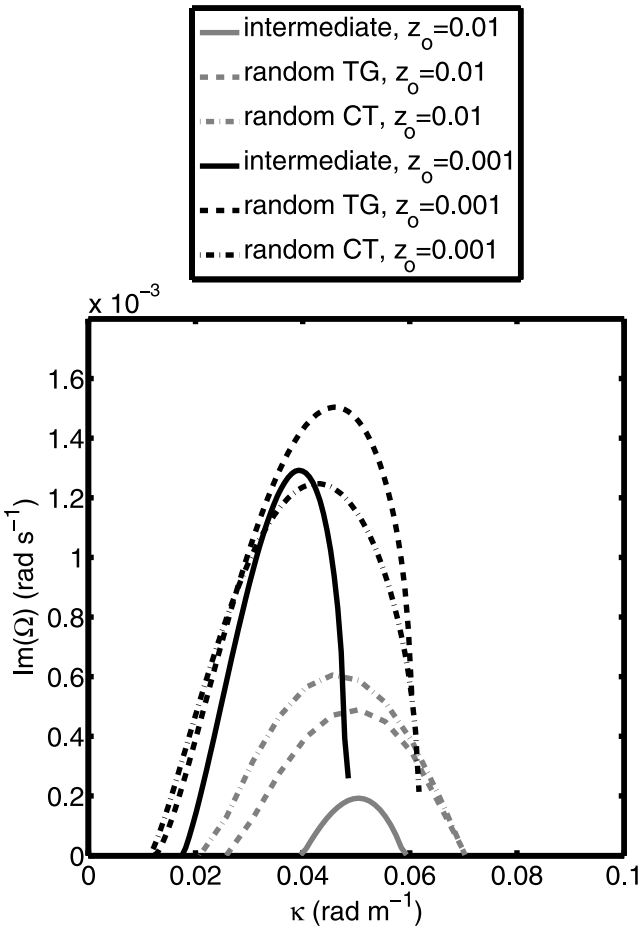

Figure 4. Rip current growth rate curves for different wave types, i.e., intermediate and random (both *Thornton and Guza* [1983] (TG) and *Church and Thornton* [1993] (CT) cases) with no feedback of perturbations on $\mathcal{D}$ for $H_{rmso\infty}$ = 1.5 m, T = 10 s, β = 0.07, and M = 0.5 and for bed roughness lengths z_o = 0.001 m and z_o = 0.01 m.

2.2. Linear Stability Analysis

[21] The standard practice of linear stability analysis is to first define a basic state, which is a time-invariant solution to the equations. The stability of this basic state is then analyzed by superimposing periodic perturbations and then linearizing with respect to the perturbations. In the basic state an alongshore uniform beach, $z_b = -\beta x$ is assumed, with the basic state variables u_o = 0, v_o = 0 (since we are considering normal incidence), $z_s = z_{so}(x)$, $E = E_o(x)$ and $\Phi = \Phi_o(x)$ (the subscript o denotes basic state terms; note that we do not use it for z_b, which is kept fixed throughout).

[22] The basic state variables are found by integrating onshore the basic state equations (1), (2), (3), and (4), thus determining the shoreline position with a prescribed tolerance depth of $D_o(0)$ = 15 cm, which is used throughout this study to avoid numerical problems. H_{rmso} and the wave period, T are prescribed in deep water (offshore) conditions.

Table 1. Rip Spacing L, e-Folding Time T_e, and Maximum Growth Rate Ω_i for FGM for Different Wave Types, With No Perturbation on $\mathcal{D}$[a]

	L (m)			T_e (min)			Ω_i (10^{-3} s^{-1})		
Intermediate	138	158	124	6.17	12.93	87	2.7	1.3	0.19
Random TG	115	137	124	6.22	11.1	34	2.7	1.5	0.49
Random CT	130	147	138	8.77	13.37	28	1.9	1.2	0.61
M	0	0.5	0.5	0	0.5	0.5	0	0.5	0.5
z_o (cm)	0.1	0.1	1	0.1	0.1	1	0.1	0.1	1

[a] $H_{rmso\infty} = 1.5$ m, $T = 10$ s, $\beta = 0.07$, Reynolds stresses turned on and off through M, and bottom friction increased through the increase in z_o.

[23] The basic state variables plus perturbations are

$$
\begin{aligned}
z_s &= z_{so}(x) + z_s'(x)\exp[i(\kappa y - \Omega t)],\\
u &= u'(x)\exp[i(\kappa y - \Omega t)],\\
v &= v'(x)\exp[i(\kappa y - \Omega t)],\\
E &= E_o(x) + e'(x)\exp[i(\kappa y - \Omega t)],\\
\Phi &= \Phi_o(x) + \phi'(x)\exp[i(\kappa y - \Omega t)],
\end{aligned}
\tag{12}
$$

where the eigenvalue $\Omega = \Omega_r + i\Omega_i$ and κ is the radian wave number, indicating the spatial periodicity in the alongshore direction. Thus, for a given spacing (wavelength) $L = 2\pi/\kappa$, the growth (or decay) rate of the resulting eigenfunction $[z_s', u', v', e', \phi']^T$ is given by Ω_i, with corresponding e-folding time $T_e = \Omega_i^{-1}$, and the (alongshore) propagation velocity is given by Ω_r/κ. The eigenfunction (mode) with the largest growth rate is considered to be the one that will be seen in nature: the fastest growing mode or FGM. The resulting linear stability equations thus define an eigenvalue problem, which is solved using collocation methods, with the perturbations decaying to zero far offshore [see *Calvete et al.*, 2005]. The shoreline is taken to be fixed at $x = 0$, with a basic state shoreline depth of 15 cm. The amplitude of all perturbed variables is arbitrary. When $M \neq 0$ (Reynolds stress terms included) $u' = v' = 0$ at $x = 0$; when $M = 0$ (Reynolds stress terms excluded) $u'(x = 0) = 0$. Numerical experiments here were performed for 250 grid points with half the grid points within 300 m of the shoreline, for which settings numerical convergence was achieved.

3. Generation of Rip Currents

[24] We examine a plane sloping beach with beach slope $\beta = 0.07$, chosen because it was used by *Yu* [2006]. The beach profile here extends to 4 km offshore (where $D_0 = 280$ m, so that deep water conditions pertain and we can expect perturbations to be negligible), after which a constant depth is assumed. The beach is thus, for practical purposes, plane. A similar profile was taken by *Yu* [2006]; however, the constant depth section began after 45.76 m ($D_0 = 3.2$ m), so shallow water conditions were assumed everywhere.

[25] The default value for offshore H_{rmso} is $H_{rmso\infty} = 1.5$ m, with period $T = 10$s following *Yu* [2006]; this was also the approximate observed period on Narrabeen beach, Australia [see *Short*, 1985]. Unlike previous studies, where Reynolds stress was neglected, we include these terms, although, because we consider normal incidence, turbulent diffusivity and bottom friction are not present in the basic state. The basic states for the different wave dissipations can be seen in Figure 2.

[26] Results are roughly as expected. There is increased set-up for intermediate waves, which break later, therefore

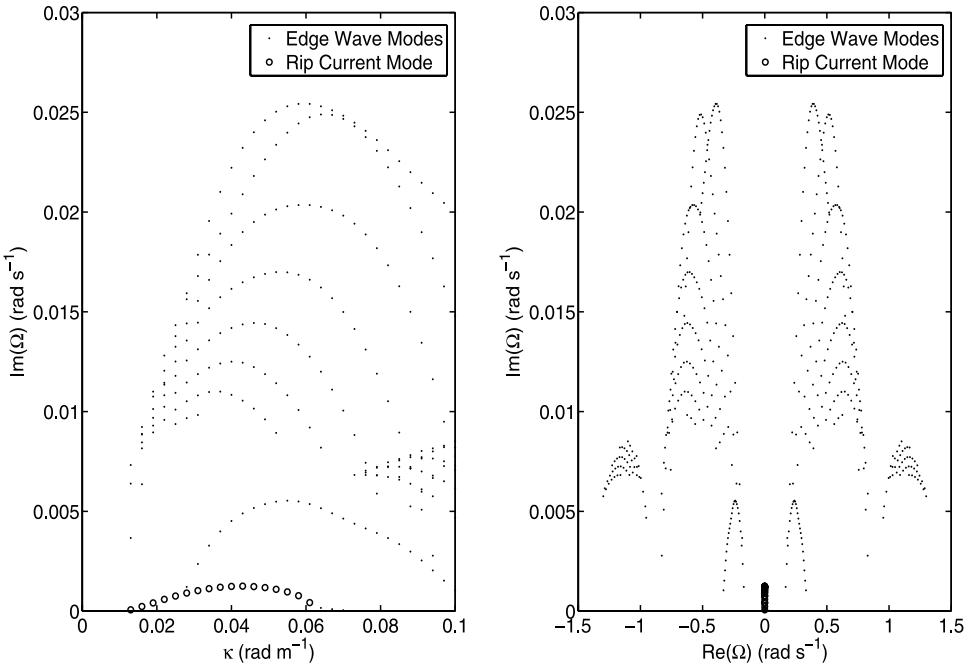

Figure 5. (left) Growth rate curves for edge wave and rip current modes. (right) Frequency versus growth rate curves for edge wave and rip current modes. Both are for *Thornton and Guza* [1983] waves with no feedback of perturbations on $\mathcal{D}$ for $H_{rmso\infty} = 1.5$ m, $T = 10$ s, $\beta = 0.07$, $z_o = 0.001$ m, and $M = 0.5$.

allowing more shoaling prior to breaking and therefore larger set-down. The maximum breaker height decreases and moves offshore as waves become more random, thus resulting in the reduction in set-up. Note also in Figure 2 the differences in the dissipation: with delayed breaking the dissipation in the inner surf zone is higher because the same offshore wave energy density must be dissipated in a shorter distance.

[27] An integration from the shore to deep water shows that the quantity $-\int_0^\infty \mathcal{D}dx + Ec_g|_{D=D(\text{shore})}$ must be equal for all formulas (in the basic state), and this provides a useful check on the model. It turns out that $\mathcal{D}$ plays a crucial role in determining whether or not instabilities develop, and for this reason, in sections 3.1 and 3.2 we isolate this physics by first excluding it in the perturbation equations (i.e., we neglect the feedback of the perturbations on this term), consistent with *Falqués et al.* [1999] and *Yu* [2006], and then reincorporate it into the full equations (1)–(4).

3.1. No Feedback of Perturbations Onto Dissipation

[28] Figures 3 and 4 show the growth rate curves for different basic state $\mathcal{D}$ terms (excluding feedback, as previously mentioned) when turbulent Reynolds stresses are turned off and on, and when bottom friction is increased through the increase in bed roughness length, z_o. The predicted rip spacing and the FGM e-folding time ($T_e = 1/\Omega_i$) (the time taken for the rip currents to grow a factor of e) are shown in Table 1. Figure 3 shows the reduction in growth rates when the turbulent Reynolds stress term is included. Figure 3 (left) also shows the detailed structure of the growth rate curves. It can be seen that two imaginary modes (for instance, mode 1a and mode 1b) merge to form a complex conjugate solution (mode 1), the solutions to which have equal growth and migration rate magnitudes but are migrating in opposite directions. The bifurcation behavior seen here is similar to that given by *Van Leeuwen et al.* [2006], who investigated morphodynamical instabilities on a plane sloping beach. Here, we only consider the fastest growing imaginary mode, i.e., mode 1a. The alongshore propagating complex conjugate modes, by themselves, are not expected to correspond to physical rip currents (because of the migration). Note that if these two modes were to possess equal amplitudes, however, the result is a standing wave solution. We nevertheless exclude this solution, because it would comprise a reversing onshore and offshore propagating rip current mode, which is also nonphysical. Note also that the inclusion of the Reynolds stresses minimizes the range of wave numbers over which these complex conjugate solutions exist, and also reduces their growth rates. Furthermore, the unstable complex conjugate solutions are no longer present for increased bottom friction. Similarly, when bed friction is increased, growth rates are reduced: see Figure 4. The observed damping effect of Reynolds stress and bed friction terms on growth rates of rip currents is consistent with other kinds of instability studies (e.g., the shear wave studies by *Dodd et al.* [1992] and *Falqués and Iranzo* [1994]).

[29] When Reynolds stress terms are included, the peak of the growth rate curve shifts toward larger rip spacing, consistent with greater diffusion; the opposite is true for increased bottom friction. Figures 3 and 4 also indicate that rip spacings are slightly higher for intermediate waves, which have a higher shoreline basic state setup (see Figure 2a).

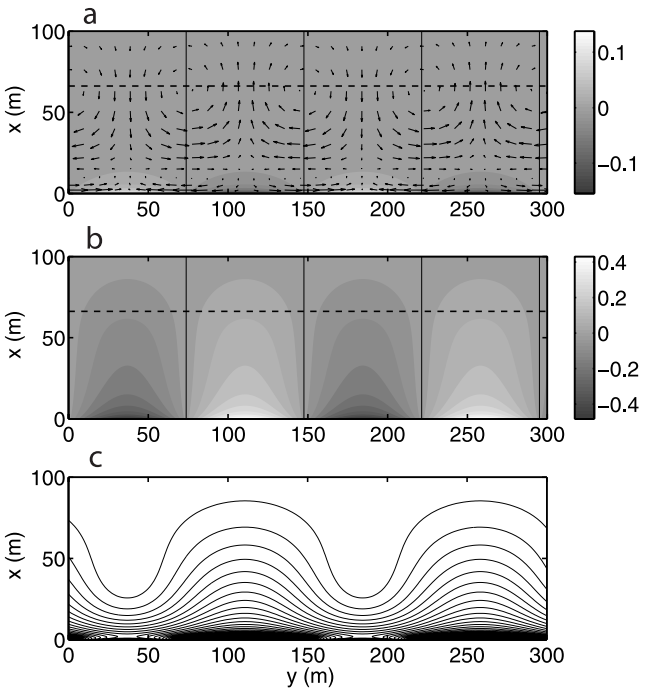

Figure 6. Flow pattern and structure of FGM in Figure 3 for *Church and Thornton* [1993] dissipation and when turbulent Reynolds stress is included. No feedback is shown of perturbation onto dissipation. (a) Mean free surface elevation (z_s') and flow perturbation ($\vec{u}'$). Elevation (depression) is denoted by light (dark) colors and flow pattern shown by arrows. (b) Wave energy perturbations (e'). High (low) energy is denoted by light (dark) areas. (c) Perturbed wavefronts (ϕ', lines of equal phase). The thin solid black line in Figures 6a and 6b is the zero contour; the thick black horizontal dashed line shows the maximum basic state wave energy dissipation.

[30] It is instructive to examine the position of these growing modes in relation to other hydrodynamical complex conjugate modes, in particular edge waves. Figure 5 shows the growth rate curves for growing rip and edge wave modes, which emerge from the same conditions, and the real and imaginary parts of the these eigenvalues. Figure 5 clearly shows the larger growth rates for the edge wave modes, and the mainly non-propagating nature of the rip current mode. We remark on this in the discussion. Previous studies [e.g., *Howd et al.*, 1992; *Falqués et al.*, 2000], who examine edge waves in the presence of an alongshore current) typically assume a real phase speed, thus ruling out the possibility of growth.

[31] Figure 6 shows a growing rip cell for the FGM (for *Church and Thornton* [1993] dissipation) and is typical of those for the other dissipations: see Figures 7 and 8. Two circulation cells can be seen in Figures 6–8, one very close to the shore (and small in extent): the "shoreline cell", and the other farther offshore and larger, spanning the surf zone (and therefore being more characteristic of rip-current circulations): the "surf zone cell". The shoreline cell has the opposite circulation to that that might be expected: i.e., flow from regions of lower setup to regions of higher setup in the alongshore direction as shown by *Calvete et al.* [2005]. *Yu*

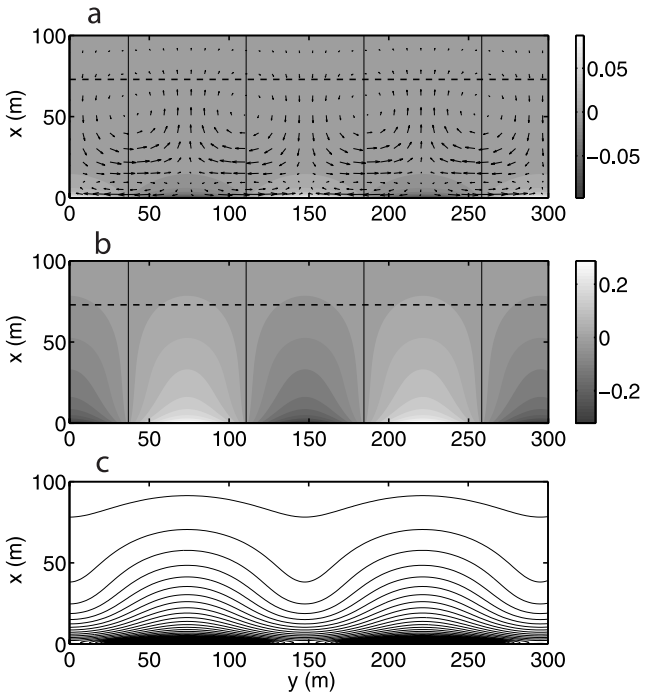

Figure 7. Flow pattern and structure of FGM in Figure 3 for *Thornton and Guza* [1983] dissipation and when turbulent Reynolds stress is included. No feedback is shown of perturbation onto dissipation. (a) Mean free surface elevation (z_s') and flow perturbation ($\vec{u}'$). Elevation (depression) is denoted by light (dark) colors, and flow pattern is shown by arrows. (b) Wave energy perturbations (e'). High (low) energy is denoted by light (dark) areas. (c) Perturbed wavefronts (ϕ', lines of equal phase). The thin solid black line in Figures 7a and 7b is the zero contour; the thick black horizontal dashed line shows the maximum basic state wave energy dissipation.

and Slinn [2003] also observe these circulations, although it is not clear which are regions of high or low setup in their study. Note, however, that for *Calvete et al.* [2005], both for fixed and mobile beds, the set-up at the shore is opposite to that observed here; that is, it is negative where there is offshore flow in the shoreline cell, although the set-up quickly reverses sign at these locations just a little further offshore. There are, however, significant differences between the present study and that of *Calvete et al.* [2005], who examined a barred beach with mean slope less than $\beta = 0.07$ with an alongshore bar. Moreover, the shoreline cells they observe are less energetic compared to the surf zone cells they observe. Further, it must be remembered that here we exclude feedback onto wave dissipation. Thus, the rip currents here do not induce further breaking, as they did for *Calvete et al.* [2005], but only shoaling and refraction. Thus, for *Calvete et al.* [2005], where wave heights are larger in the rip channels because of the larger depth there, there is intense breaking at the corresponding shoreline position of the channel locations, and therefore a large set-up there. In contrast, offshore flows in the cells considered here also lead to increased wave heights, because of shoaling, but there is no associated breaking, so set-up decreases. Shoreline cells have also been observed in laboratory experiments by *Haller et al.* [2002] and *Haas and Svendsen* [2002].

[32] Within the larger rip current cell the water flows alongshore from regions of higher setup (where wave height is lowest) to regions of lower setup characteristic of the classical rip cell. The major difference observed regarding the shoreline cells for the different dissipations is their strength relative to the surf zone circulation, which is largest for intermediate waves. This suggests that as waves become more regular shoreline cells extend further offshore and become more dominant. This is a result of the increased wave energy dissipation over a shorter distance.

[33] The wave energy perturbation (see Figures 6, 7, and 8), like setup, retains the same sign in shoreline and surf zone cells and reaches a peak at the shoreline, contrary to the cells of *Yu* [2006], which reach a peak at the breaker line. The physics of patterns shown here can be understood by noting that the increase (decrease) in wave energy toward the shore with respect to the basic state results in an overall diminution (increase) of the force ($\frac{\partial S_{11}}{\partial x}$) driving the setup, which therefore amounts to an offshore (onshore) directed force, resulting in offshore (onshore) current and a decrease (increase) in set-up, as is observed.

[34] Considering now a region of shoreward decreasing, negative e', the extra onshore force thus drives a current

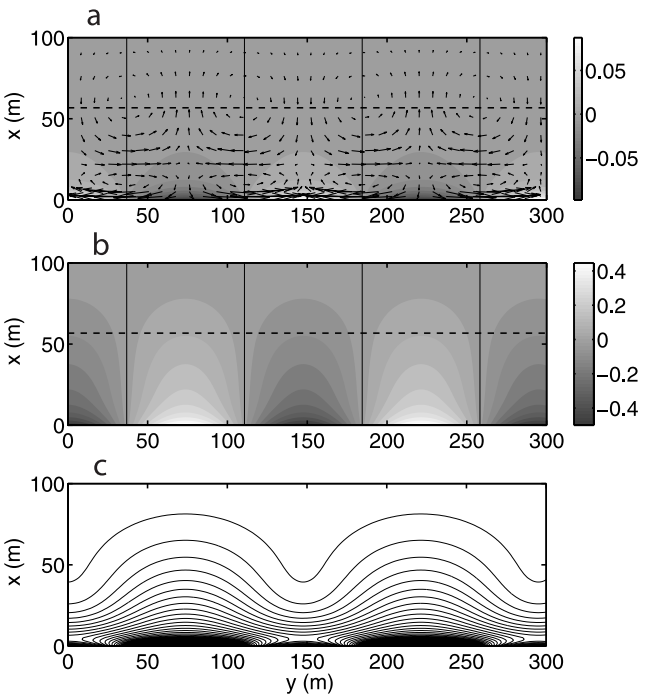

Figure 8. Flow pattern and structure of FGM in Figure 3 for intermediate waves and when turbulent Reynolds stress is included. No feedback is shown of perturbation onto dissipation. (a) Mean free surface elevation (z_s') and flow perturbation ($\vec{u}'$). Elevation (depression) is denoted by light (dark) colors, and flow pattern is shown by arrows. (b) Wave energy perturbations (e'). High (low) energy is denoted by light (dark) areas. (c) Perturbed wavefronts (ϕ', lines of equal phase). The thin solid black line in Figures 8a and 8b is the zero contour; the thick black horizontal dashed line shows the maximum basic state wave energy dissipation.

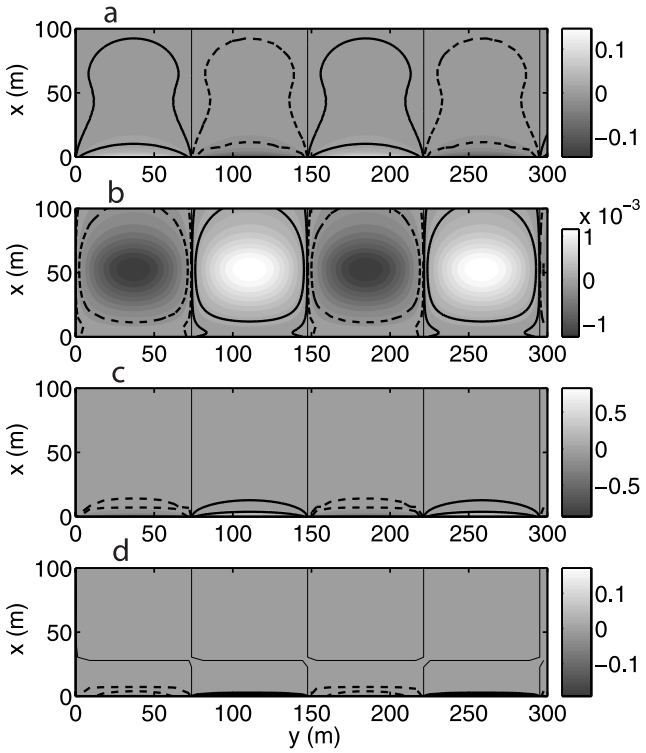

Figure 9. (a) $S_{11,x}$, (b) $S_{12,y}$, (c) $gz_{s,x}$, and (d) $gz_{s,x} + S_{11,x}/\rho D + S_{12,y}/\rho D$ for *Church and Thornton* [1993] results as seen in Figure 6. Thin lines are the zero contour. Thick solid lines are the 1% and 10% of maximum contours. Broken lines are the equivalent contours for negative values.

onshore. This onshore current is opposed by the increased set-up gradient at the shore that accompanies the increased wave energy dissipation; this comprises a negative feedback. To understand the positive feedback necessary for the instability we must consider the shoaling and refraction. This onshore current will effectively increase c_g (because $c_g + U > c_g$) and so deshoal the wave, thus further decreasing e' and moving the break point onshore. Furthermore, the onshore current de-focuses the waves, thus also providing a positive feedback; this effect can be seen in the lines of equal phase in Figure 6, 7, and 8). In the surf zone this effect will be felt as (1) a decrease in e' due to the deshoaling, which provides a positive feedback, and (2) a decrease in breaking (because of decreased wave height), thus providing a negative feedback because reduced breaking will increase wave heights. This is the very term that we omit here, and we know its effect to be strong because it "kills" the growing cell (i.e., renders it stable): see section 3.2.

[35] The rest of the two cell dynamics can be understood from Figures 9 and 10 (which are for *Church and Thornton* [1993] dissipation and are similar for those for other dissipations). Consider first the surf zone cells: we can see that (see also Figure 6) where wave height is increased, forcing is indeed offshore, because of $S_{11,x}$. $S_{12,y}$ is positive in regions of offshore current, therefore providing an onshore force due to pure focusing of wave direction by refraction on the current. Note that the local increase in wave energy that accompanies this focusing, and which provides a positive feedback, occurs at second order, and so is absent here. However, $|S_{12,y}| \ll |S_{11,x}|$ everywhere, so the cross-shore positive feedback mechanism prevails. In contrast, the dominant alongshore radiation stresses oppose this circulation pattern, because the increased wave heights lead to larger $S_{22,y}$ either side of these regions, which would drive opposing currents ($|S_{12,x}| \ll |S_{22,y}|$ everywhere). However, in these regions alongshore gradients in set-up overcome these opposing forces and so drive the feeder currents alongshore in the region approximately 10 m $< x <$ 65 m. Seaward of 65 m radiation stresses prevail and the water is recirculated in the surf zone cells. Although small, $S_{12,x}$ is important in reinforcing $S_{22,y}$ offshore.

[36] At the shore, $|S_{22,y}/\rho D| > g|\partial z_s/\partial y|$, and so water is driven against the alongshore set-up gradient and driven offshore by the cross-shore set-up gradient, which locally exceeds the onshore force because of the cross-shore radiation stress gradients, which drive the surf zone cell onshore in regions of diminished wave height, in the region approximately $x <$ 30 m. This water then recirculates alongshore because of the same radiation stress gradients that drive the nearshore alongshore part of the surf zone cell and then return shoreward because of diminished set-up gradient.

[37] So, the positive feedback appears to stem from the surf zone cell circulation, which therefore is a free instability. The shoreline circulation therefore appears as a forced circulation, consistent with the conclusion of *Calvete et al.* [2005]. Note also that the feedback mechanism requires refraction and shoaling and, moreover, that these effects be operational in the surf zone. For purely depth-limited waves this will not happen, so we may expect a weaker feedback for the intermediate waves, compared to the forced shore-

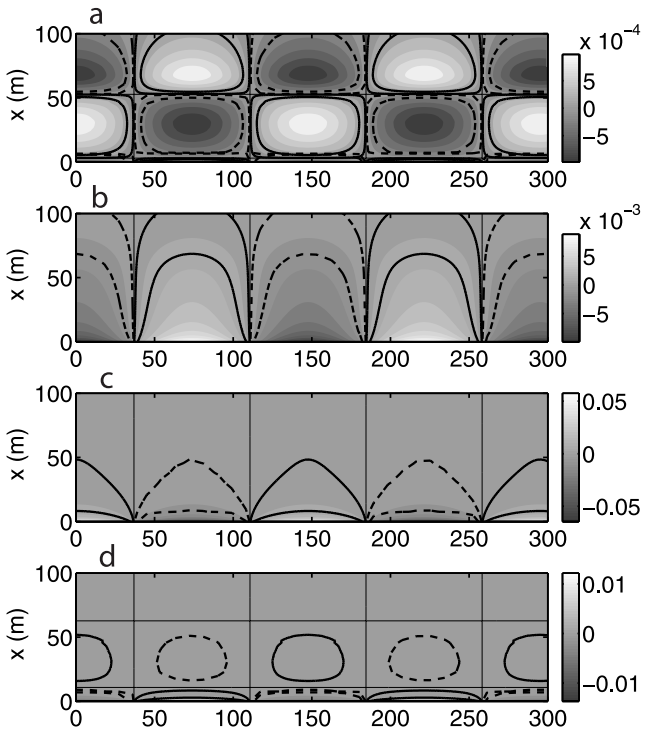

Figure 10. (a) $S_{12,x}$, (b) $S_{22,y}$, (c) $gz_{s,y}$, and (d) $gz_{s,y} + S_{12,x}/\rho D + S_{22,y}/\rho D$ for *Church and Thornton* [1993] results as seen in Figure 6. Thin lines are the zero contour. Thick solid lines are the 1% and 10% of maximum contours. Broken lines are the equivalent contours for negative values.

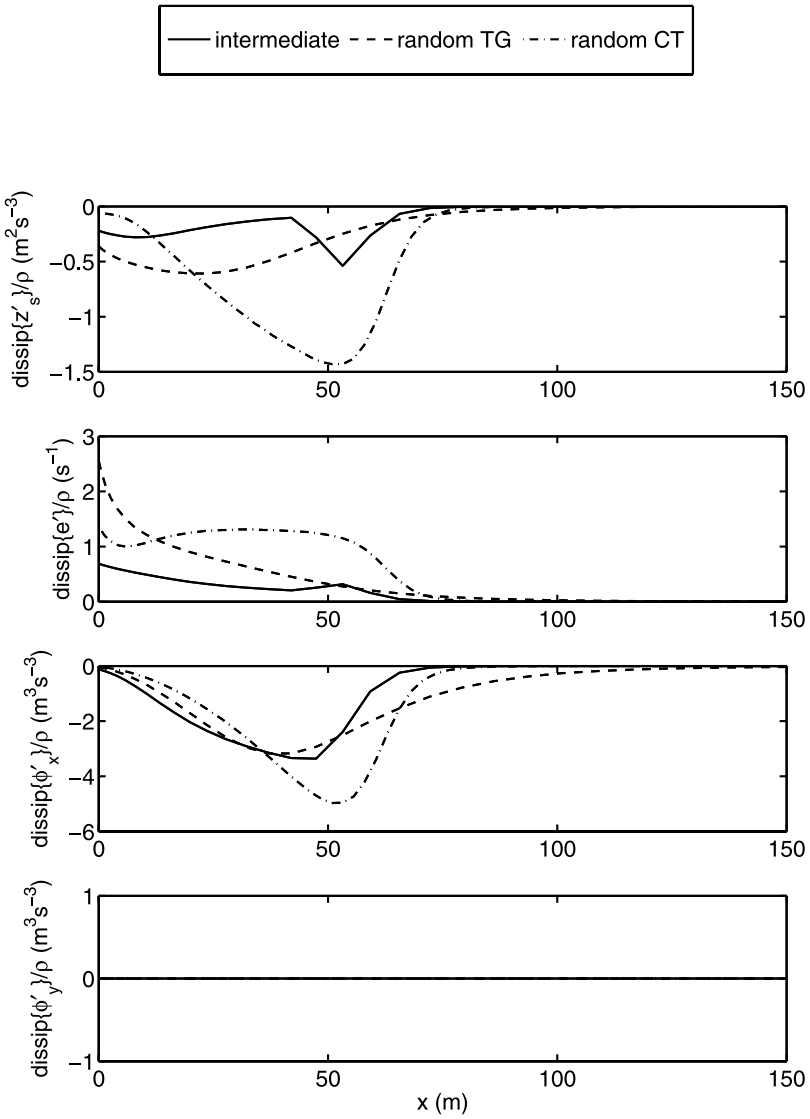

Figure 11. Cross-shore structure of $\mathcal{D}\{z'_s\}$, $\mathcal{D}\{e'\}$, and $\mathcal{D}\{\phi'_{,l}\}$ for intermediate and random (both *Thornton and Guza* [1983] (TG) and *Church and Thornton* [1993] (CT) cases).

line cells, which are directly driven by gradients in wave height and set-up.

[38] In the study of *Yu* [2006], the maximum wave energy was concentrated around the breaker line, but the surf zone was depth controlled, which also has implications for the feedback onto the dissipation, which we ignore in this section: see section 3.2.

[39] Finally, Figures 6, 7, and 8 also show the perturbed wavefronts. They show similar characteristics to the perturbed wavefronts found by *Falqués et al.* [1999]. Where the rips exists there is a retarding of the wavefront, with the opposite effect where there is an onshore flow; that is, the waves shoal and refract on the currents. The aforementioned additional forcing due to refraction is therefore clearly evident [see *Falqués et al.*, 1999].

3.2. Feedback of Perturbations Onto Dissipation

[40] In section 3.1, we did not include perturbations in the wave energy dissipation due to wave breaking when analyzing the formation of circulation cells. So, the growing cells are influenced by refraction and shoaling only, and have no direct feedback on to wave breaking. The perturbation expansion with respect to depth, energy and phase of the wave energy dissipation can be written like:

$$\frac{\partial e'}{\partial t} + \ldots = -\mathcal{D} = -\mathcal{D}\{z'_s\}z'_s - \mathcal{D}\{e'\}e' - \mathcal{D}\left\{\phi'_{,l}\right\}\phi'_{,l} \qquad (13)$$

where the terms $\mathcal{D}\{\}$ indicate basic state terms, whose form depends on the dissipation used, l = 1, 2, and $\mathcal{D}\{\phi'_{,l}\}\phi'_{,l} = \mathcal{D}\{\partial_x\phi'\}\partial_x\phi' + \mathcal{D}\{\partial_y\phi'\}\partial_y\phi'$. The details on the derivation of $\mathcal{D}\{\}$ for the three dissipation formula are given in Appendix A.

[41] All the terms in (13) provide negative feedback for the incipient cells: see Figure 11. It is clear from Figure 11 (and (13)) that the feedback of the wave height onto the growing circulation cells is negative. In fact, this feedback is dominant, as seen in Figure 12, in which we see growth

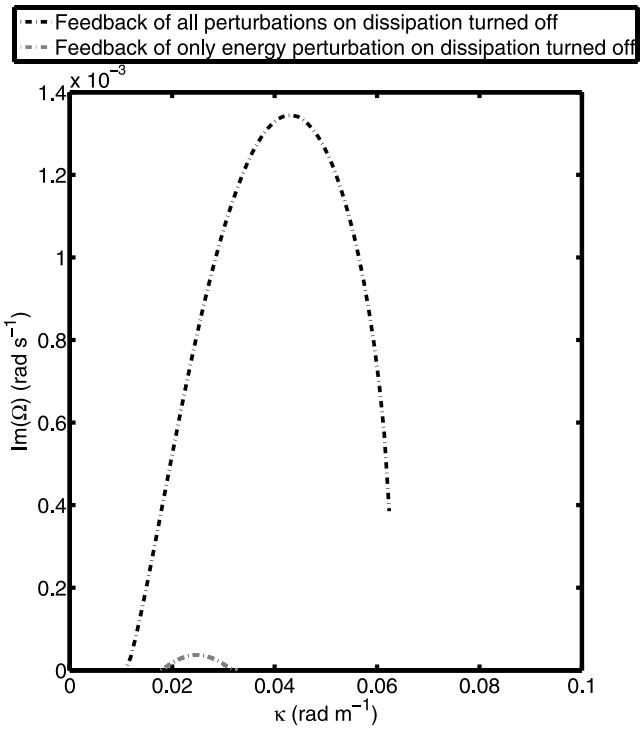

Figure 12. Circulation cell growth rate curves for *Church and Thornton* [1993] (CT) random wave dissipation (black line) with no feedback of perturbation onto $\mathcal{D}$ (i.e., $\mathcal{D}\{e'\} = \mathcal{D}\{z_s'\} = \mathcal{D}\{\phi'_{,l}\} = 0$) and (grey line) excluding only $\mathcal{D}\{e'\}$ (i.e., $\mathcal{D}\{e'\} = 0$).

rate curves without any dissipation feedback (cf. Figure 3), and including $\mathcal{D}\{z_s'\}$ and $\mathcal{D}\{\phi'_{,l}\}$ only, in which case the growth rate is reduced but the cells still are unstable. Including $\mathcal{D}\{e'\}$, with or without the other dissipation terms, leads to stability.

4. Discussion and Conclusions

[42] The results obtained here point to the existence of a positive feedback mechanism that is purely hydrodynamical that can drive rip cells; this is consistent with previous studies. This mechanism, however, does not exist when the surf zone is not saturated, because negative feedback provided by increased (decreased) breaking for positive (negative) wave energy perturbations overwhelms the shoaling/refraction mechanism. This is true regardless of what kind of random wave dissipation is considered or if intermediate waves are considered.

[43] All the non-regular wave dissipations examined here give rise to these hydrodynamical instabilities when feedback onto dissipation is neglected, and all also give rise to two cells, surf zone and shoreline, which have opposing circulations. The positive feedback mechanism is due to (de)shoaling on the (onshore) offshore current and is therefore more dominant further offshore, in the surf zone cell; alongshore, in the surf zone, set-up gradients drive them. The shoreline cells are driven by alongshore wave-generated forces because of the wave height field induced by the positive feedback mechanism, and offshore/onshore by large cross-shore set-up gradients at the shore, again induced by the positive feedback mechanism further offshore. These rip cells occupy a distinct region of frequency/wave number space, and are easily distinguished from edge waves, and indeed shear waves.

[44] Results show that the dominant effect that destroys these hydrodynamical instabilities is the feedback of the wave energy onto the dissipation (as opposed to the lesser effects of feedback of mean free surface and phase, which are also negative). The conclusion is that the effect is a strong one—indeed, the corresponding term (see (13)) must be reduced by a factor of the order of 0.01 to allow the instability mechanism to prevail. The implication of this is that the effect is strong and will not allow hydrodynamical instabilities to grow for random seas.

[45] This does not, however, preclude the possibility of a hydrodynamical instability, like that of *Yu* [2006], developing on a beach where wave heights are truly saturated. As noted earlier [*MacMahan et al.*, 2006], field data does not at present help to resolve this issue. The growing cells of *Yu* [2006] also show some qualitative differences from those we observe, in particular the peak in the wave height, which appears to be at the breaker line, in contrast to ours, which is at the shoreline. Note, however, that *Yu* [2006] considers strictly regular, depth-limited waves, imposes a moving shoreline and also has strictly shallow water wave transformation, all of which leads to significant differences with the study we present. There is evidence, however, of a shoreline cell in the results of *Yu* [2006, Figure 10]. Note also that the imposition of strictly depth-limited regular waves means that the wave energy is slaved to the local depth, i.e., $e' = (\gamma/4)\rho g D_0 z'_s$, where γ is the breaker index, which means that the time development of wave energy perturbations is controlled through the continuity equation. There is thus no possibility of negative (or positive) feedback through the energy equation (13) (i.e., (3)), although the positive feedback we observe would still be possible in the shoaling zone. Finally, note that it is possible to construct a basic state dissipation function ($\mathcal{D}_0$), which imposes strict depth limitation at leading order. Perturbations in the resulting energy equation then may allow deviations from strict depth limitation. Studies based on this approach could prove fruitful in examining beaches close to having a saturated surf zone.

[46] Our results also indicate that edge waves may grow faster than the rip modes (when feedback onto dissipation is ignored). However, for edge waves to be responsible for rip currents two propagating modes of equal amplitude are required (i.e., a standing mode). Even then, rip growth is only a second-order effect because of interaction with the incoming wavefield and therefore not directly related to growth rate, unlike the rip modes. Furthermore, inclusion of feedback onto dissipation also damps edge modes.

[47] The stabilizing effect of random waves on rip currents found here for a non-erodible beach suggests that rip channels are more likely to appear in the field as a morphodynamical instability rather than to be driven by a hydrodynamical instability. This does not preclude the possibility that a hydrodynamical instability might develop and create rip-like features in the absence (initially at least) of a channel.

For this to happen, however, our results indicate that a saturated surf zone would be required.

Appendix A: Perturbation Terms for Different Wave Energy Dissipation $\mathcal{D}$ Models

[48] The linearization of $\mathcal{D}$ (in equation (3)) is made by using the decomposition (12); that is, each variable f is decomposed into the basic state (denoted by subscript o) and the perturbation (denoted by $'$) parts, i.e., $f = f_o(x) + f'(x)\exp[i(\kappa y - \Omega t)]$. Apart from the decompositions of variables defined in (12), we also introduce the following decompositions:

$$D = D_o(x) + z'_s(x)\exp[i(\kappa y - \Omega t)],$$

with $D_o(x) = z_{so}(x) - z_b(x)$, and,

$$\vec{K} = \vec{K}_o(x) + \vec{k}'(x)\exp[i(\kappa y - \Omega t)],$$

where $\vec{K}_o = (K_{o1}, K_{o2}) = (K_o, 0)$, with K_o, the wave number at the basic state. Each component of $\vec{K}$ can be written as ($l = 1, 2$):

$$K_l = K_{ol}(x) + \{\phi'(x)\exp[i(\kappa y - \Omega t)]\}_{,l}.$$

Thus for each of the three dissipation formula used, we can write the linearized form of $\mathcal{D}$ as

$$\mathcal{D} = \mathcal{D}\{0\} + \mathcal{D}\{z'_s\}z'_s + \mathcal{D}\{e'\}e' + \mathcal{D}\left\{\phi'_{,l}\right\}\phi'_{,l}, \tag{A1}$$

where $\mathcal{D}\{0\}$ is the basic state term for the wave energy dissipation. $\mathcal{D}\{z'_s\}$, $\mathcal{D}\{e'\}$, and $\mathcal{D}\{\phi'_{,l}\}$ include the collected terms that are coefficients of z'_s, e', and $\phi'_{,l}$, respectively, and are computed from the Taylor expansion of $\mathcal{D}$ around the basic state. The derivations of these generic basic state terms $\mathcal{D}\{\}$ for each formula are described in sections A1–A3. Moreover, we introduce Γ_o defined as

$$\Gamma_o = \left(\frac{8E_o}{\rho g}\right)^{\frac{1}{2}}\frac{1}{D_o},$$

and

$$\sigma\{0\} = gK_o\tanh(K_oD_o)^{\frac{1}{2}}.$$

A1. *Church and Thornton* [1993] Dissipation Model

[49] The formula (11) developed by *Church and Thornton* [1993] for random waves is repeated here:

$$\mathcal{D} = \frac{3\sqrt{\pi}}{16}\rho g B^3 f_p \frac{H_{rms}^3}{D}\left\{1 + \tanh\left[8\left(\frac{H_{rms}}{\gamma_b D} - 1\right)\right]\right\} \times \left[1 - \left(1 + \left(\frac{H_{rms}}{\gamma_b D}\right)^2\right)^{-5/2}\right]. \tag{A2}$$

[50] The generic basic state terms for the *Church and Thornton* [1993] formula are

$$\mathcal{D}\{0\} = \frac{3}{4}\frac{\sqrt{\pi}}{\pi}B^3\sigma\{0\}E_o\Gamma_o\left\{1 + \tanh\left[8\left(\frac{\Gamma_o}{\gamma_b} - 1\right)\right]\right\} \cdot \left(1 - \frac{1}{\left(1 + (\Gamma_o/\gamma_b)^2\right)^{5/2}}\right) \tag{A3}$$

$$\mathcal{D}\{z'_s\} = \frac{3}{4}\frac{\sqrt{\pi}}{\pi}B^3\sigma\{0\}E_o\Gamma_o\left\{1 + \tanh\left[8\left(\frac{\Gamma_o}{\gamma_b} - 1\right)\right]\right\} \times \left\{(K_oD_o\ \mathrm{cosech}(2K_oD_o) - 1) \cdot \left(1 - \frac{1}{\left(1 + (\Gamma_o/\gamma_b)^2\right)^{5/2}}\right) - 5\frac{(\Gamma_o/\gamma_b)^2}{\left(1 + (\Gamma_o/\gamma_b)^2\right)^{7/2}} - 8\left(\frac{\Gamma_o}{\gamma_b}\right)\left\{1 - \tanh\left[8\left(\frac{\Gamma_o}{\gamma_b} - 1\right)\right]\right\} \times \left(1 - \frac{1}{\left(1 + (\Gamma_o/\gamma_b)^2\right)^{5/2}}\right)\right\}\frac{1}{D_o} \tag{A4}$$

$$\mathcal{D}\{e'\} = \frac{3}{4}\frac{\sqrt{\pi}}{\pi}B^3\sigma\{0\}E_o\Gamma_o\left\{1 + \tanh\left[8\left(\frac{\Gamma_o}{\gamma_b} - 1\right)\right]\right\} \times \left\{1.5\left(1 - \frac{1}{\left(1 + (\Gamma_o/\gamma_b)^2\right)^{5/2}}\right) + 2.5\frac{(\Gamma_o/\gamma_b)^2}{\left(1 + (\Gamma_o/\gamma_b)^2\right)^{7/2}} + 4\left(\frac{\Gamma_o}{\gamma_b}\right)\left\{1 - \tanh\left[8\left(\frac{\Gamma_o}{\gamma_b} - 1\right)\right]\right\} \times \left(1 - \frac{1}{\left(1 + (\Gamma_o/\gamma_b)^2\right)^{5/2}}\right)\right\}\frac{1}{E_o} \tag{A5}$$

$$\mathcal{D}\left\{\phi'_{,l}\right\} = \frac{3}{4}\frac{\sqrt{\pi}}{\pi}B^3\sigma\{0\}E_o\Gamma_o\left\{1 + \tanh\left[8\left(\frac{\Gamma_o}{\gamma_b} - 1\right)\right]\right\} \times \left[\left(1 - \frac{1}{\left(1 + (\Gamma_o/\gamma_b)^2\right)^{5/2}}\right)(0.5 + K_oD_o\ \mathrm{cosech}(2K_oD_o))\right]\frac{K_{ol}}{K_o^2} \tag{A6}$$

A2. *Thornton and Guza* [1983] Dissipation Model

[51] The formula developed by *Thornton and Guza* [1983] is also valid for random waves, it reads

$$\mathcal{D} = \frac{3\sqrt{\pi}}{16}B^3 f_p \rho g \frac{H_{rms}^5}{\gamma_b{}^2 D^3}\left(1 - \frac{1}{\left(1 + (H_{rms}/\gamma_b D)^2\right)^{5/2}}\right). \tag{A7}$$

The generic basic state terms for *Thornton and Guza* [1983] formula are

$$\mathcal{D}\{0\} = \frac{3}{4}\sqrt{\pi}\pi B^3\sigma\{0\}E_o\frac{\Gamma_o^3}{\gamma_b{}^2}\left(1 - \frac{1}{\left(1 + (\Gamma_o/\gamma_b)^2\right)^{5/2}}\right), \tag{A8}$$

$$\mathcal{D}\{z_s'\} = -\frac{3}{4}\frac{\sqrt{\pi}}{\pi}B^3\sigma\{0\}E_o\frac{\Gamma_o^3}{\gamma_b{}^2} \times \left((3 - K_oD_o\ \mathrm{cosech}(2K_oD_o)\right) \times \left(1 - \frac{1}{\left(1+(\Gamma_o/\gamma_b)^2\right)^{5/2}}\right) + 5\frac{(\Gamma_o/\gamma_b)^2}{\left(1+(\Gamma_o/\gamma_b)^2\right)^{7/2}}\Bigg)\frac{1}{D_o}, \quad \text{(A9)}$$

$$\mathcal{D}\{e'\} = \frac{3}{4}\frac{\sqrt{\pi}}{\pi}B^3\sigma\{0\}E_o\frac{\Gamma_o^3}{\gamma_b{}^2}\left(\frac{5}{2}\left(1 - \frac{1}{\left(1+(\Gamma_o/\gamma_b)^2\right)^{5/2}}\right) + \frac{5}{2}\frac{(\Gamma_o/\gamma_b)^2}{\left(1+(\Gamma_o/\gamma_b)^2\right)^{7/2}}\right)\frac{1}{E_o}, \quad \text{(A10)}$$

$$\mathcal{D}\left\{\phi_{,l}'\right\} = \frac{3}{4}\frac{\sqrt{\pi}}{\pi}B^3\sigma\{0\}E_o\frac{\Gamma_o^3}{\gamma_b{}^2}\left(1 - \frac{1}{\left(1+(\Gamma_o/\gamma_b)^2\right)^{5/2}}\right) \times (0.5 + K_oD_o\ \mathrm{cosech}(2K_oD_o))\frac{K_{ol}}{K_o^2}. \quad \text{(A11)}$$

A3. *Van Leeuwen et al.* [2006] Dissipation Model

[52] The formula developed by *Van Leeuwen et al.* [2006] can be used for depth-limited regular, regular and intermediate waves, depending on the value chosen for m and n. It reads

$$\mathcal{D} = \frac{\rho g f_p B^3 H_{rms}^3}{4D}\left(\frac{H_{rms}}{\gamma_b D}\right)^m\left\{1 - \exp\left[-\left(\frac{H_{rms}}{\gamma_b D}\right)^n\right]\right\}. \quad \text{(A12)}$$

In the paper we set $m = 0$ and $n = 10$, which represent intermediate waves [*Van Leeuwen et al.*, 2006]. The generic basic state terms for the *Van Leeuwen et al.* [2006] formula are

$$\mathcal{D}\{0\} = \frac{B^3\sigma\{0\}E_o\Gamma_o}{\pi}\left(\frac{\Gamma_o}{\gamma_b}\right)^m\left[1 - \exp\left[-\left(\frac{\Gamma_o}{\gamma_b}\right)^n\right]\right], \quad \text{(A13)}$$

$$\mathcal{D}\{z_s'\} = -\frac{B^3\sigma\{0\}E_o\Gamma_o}{\pi}\left(\frac{\Gamma_o}{\gamma_b}\right)^m\left[n\left(\frac{\Gamma_o}{\gamma_b}\right)^n\exp\left[-\left(\frac{\Gamma_o}{\gamma_b}\right)^n\right] - \left(1 - \exp\left[-\left(\frac{\Gamma_o}{\gamma_b}\right)^n\right]\right) \times (K_oD_o\ \mathrm{cosech}(2K_oD_o) - (m+1))\right]\frac{1}{D_o}, \quad \text{(A14)}$$

$$\mathcal{D}\{e'\} = \frac{B^3\sigma\{0\}E_o\Gamma_o}{\pi}\left(\frac{\Gamma_o}{\gamma_b}\right)^m\left[0.5n\left(\frac{\Gamma_o}{\gamma_b}\right)^n\exp\left[-\left(\frac{\Gamma_o}{\gamma_b}\right)^n\right] + \left(1 - \exp\left[-\left(\frac{\Gamma_o}{\gamma_b}\right)^n\right]\right)(1.5 + 0.5m)\right]\frac{1}{E_o}, \quad \text{(A15)}$$

$$\mathcal{D}\left\{\phi_{,l}'\right\} = \frac{B^3\sigma\{0\}E_o\Gamma_o}{\pi}\left(\frac{\Gamma_o}{\gamma_b}\right)^m\left[\left(1 - \exp\left[-\left(\frac{\Gamma_o}{\gamma_b}\right)^n\right]\right) \times (0.5 + K_oD_o\ \mathrm{cosech}(2K_oD_o))\right]\frac{K_{ol}}{K_o^2}. \quad \text{(A16)}$$

[53] **Acknowledgments.** Haider Hasan was funded by an EPSRC doctoral training account award. Roland Garnier received financial support from the University of Nottingham. The authors gratefully acknowledge this support. The authors thank two anonymous reviewers for helpful comments and also thank Albert Falqués and Daniel Calvete of Applied Physics Department, Universitat Politecnica de Catalunya, for useful discussions concerning this manuscript.

References

Battjes, J. A. (1975), Modeling of turbulence in the surf zone, in *Modeling Techniques*, vol. 2, pp. 1050–1061, Am. Soc. of Civ. Eng., New York.

Bowen, A. J. (1969), Rip currents: 1. Theoretical investigations, *J. Geophys. Res.*, *74*, 5467–5478.

Bowen, A. J., and D. I. Inman (1969), Rip currents: 2. Laboratory and field observations, *J. Geophys. Res.*, *74*, 5479–5490.

Brander, R. W., and A. D. Short (2000), Morphodynamics of a large-scale rip current system at Muriwai, New Zealand, *Mar. Geol.*, *165*, 27–39.

Caballeria, M., G. Coco, A. Falqués, and D. A. Huntley (2002), Self-organization mechanism for the formation of nearshore crescentic and transverse bars, *J. Fluid Mech.*, *465*, 379–410.

Calvete, D., N. Dodd, A. Falqués, and S. M. van Leeuwen (2005), Morphological development of rip channel systems: Normal and near-normal wave incidence, *J. Geophys. Res.*, *110*, C10006, doi:10.1029/2004JC002803.

Chawla, A., and J. T. Kirby (2002), Monochromatic and random wave breaking at blocking points, *J. Geophys. Res.*, *107*(C7), 3067, doi:10.1029/2001JC001042.

Church, J. C., and E. B. Thornton (1993), Effects of breaking wave induced turbulence within a longshore current model, *Coastal Eng.*, *20*, 1–28.

Dalrymple, R. A., and C. J. Lozano (1978), Wave-current interaction for rip currents, *J. Geophys. Res.*, *83*, 6063–6071.

Damgaard, J., N. Dodd, L. Hall, and T. Chesher (2002), Morphodynamic modelling of rip channel growth, *Coastal Eng.*, *45*, 199–221.

Deigaard, R., N. Dronen, J. Fredsoe, J. H. Jensen, and M. P. Jorgesen (1999), A morphological stability analysis for a long straight barred coast, *Coastal Eng.*, *36*, 171–195.

Dodd, N., J. Oltman-Shay, and E. B. Thornton (1992), Shear instabilities in the longshore current: A comparison of observations and theory, *J. Phys. Oceanogr.*, *22*, 62–82.

Falqués, A., and V. Iranzo (1994), Numerical simulation of vorticity waves in the nearshore, *J. Geophys. Res.*, *99*, 825–841.

Falqués, A., A. Montoto, and D. Vila (1999), A note on hydrodynamic instabilities and horizontal circulation in the surf zone, *J. Geophys. Res.*, *104*, 20,605–20,615.

Falqués, A., G. Coco, and D. A. Huntley (2000), A mechanism for the generation of wave-driven rhythmic patterns in the surf zone, *J. Geophys. Res.*, *105*, 24,071–24,087.

Garnier, R., D. Calvete, A. Falqués, and M. Caballeria (2006), Generation and nonlinear evolution of shore-oblique/transverse bars, *J. Fluid Mech.*, *567*, 327–360.

Haas, K. A., and I. A. Svendsen (2002), Laboratory measurements of the vertical structure of rip currents, *J. Geophys. Res.*, *107*(C5), 3047, doi:10.1029/2001JC000911.

Haller, M. C., R. A. Dalrymple, and I. A. Svendsen (2002), Experimental study of nearshore dynamics on a barred beach with rip channels, *J. Geophys. Res.*, *107*(C6), 3061, doi:10.1029/2001JC000955.

Hino, M. (1974), Theory on the formation of rip currents and cuspidal coast, in *Coastal Engineering 1974*, pp. 901–919, Am. Soc. of Civ. Eng., New York.

Howd, P. A., A. J. Bowen, and R. A. Holman (1992), Edge waves in the presence of strong longshore currents, *J. Geophys. Res.*, *97*, 11,357–11,371.

Inman, D. L., R. T. Tait, and C. E. Nordstrom (1971), Mixing in the surf zone, *J. Geophys. Res.*, *76*, 3493–3514.

LeBlond, P. H., and C. L. Tang (1974), On the energy coupling between waves and rip currents, *J. Geophys. Res.*, *79*, 811–816.

Longuet-Higgins, M. S., and R. W. Stewart (1962), Radiation stress and mass transport in gravity waves, with application to "surf beats," *J. Fluid Mech.*, *10*, 481–504.

Longuet-Higgins, M. S., and R. W. Stewart (1964), Radiation stresses in water waves: A physical discussion, with applications, *Deep Sea Res.*, *11*, 529–562.

MacMahan, J. H., E. B. Thornton, T. P. Stanton, and A. J. H. M. Reniers (2005), RIPEX: Rip currents on a shore-connected shoal beach, *Mar. Geol.*, *218*, 113–134.

MacMahan, J. H., E. B. Thornton, and A. J. H. M. Reniers (2006), Rip current review, *Coastal Eng.*, *53*, 191–208.

Murray, A. B., and B. Reydellet (2001), A rip-current model based on a newly hypothesized interaction between waves and currents, *J. Coastal Res.*, *17*, 517–531.

Reniers, A. J. H. M., J. A. Roelvink, and E. B. Thornton (2004), Morphodynamic modeling of an embayed beach under wave group forcing, *J. Geophys. Res.*, *109*, C01030, doi:10.1029/2002JC001586.

Roelvink, J. A. (1993), Dissipation in random wave groups incident on a beach, *Coastal Eng.*, *19*, 127–150.

Shepard, F. P., and D. L. Inman (1950), Nearshore circulation related to bottom topography and wave refraction, *Eos Trans. AGU*, *31*, 555–565.

Shepard, F. P., K. O. Emery, and E. C. LaFond (1941), Rip currents: A process of geological importance, *J. Geophys. Res.*, *49*, 337–369.

Short, A. D. (1985), Rip-current type, spacing and persistence, Narrabeen beach, Australia, *Mar. Geol.*, *65*, 47–71.

Short, A. D. (1999), *Handbook of Beach and Shoreface Morphodynamics*, 1 ed., John Wiley, New York.

Short, A. D., and C. L. Hogan (1994), Rip currents and beach hazards: Their impact on public safety and implications for coastal management, *J. Coastal Res.*, *12*, 197–209.

Smith, J. A., and J. Largier (1995), Observations of nearshore circulation: Rip currents, *J. Geophys. Res.*, *100*, 10,967–10,975.

Svendsen, I. A. (2006), *Introduction to Nearshore Hydrodynamics*, *Adv. Ser. Ocean Eng.*, vol. 24, World Sci., Singapore.

Svendsen, I. A., K. Haas, and Q. Zhao (2002), Quasi-3D nearshore circulation model SHORECIRC, *Int. Rep. CACR-02-01*, Cent. for Appl. Coastal Res., Univ. of Del., Newark.

Thornton, E. B., and R. T. Guza (1983), Transformation of wave height distribution, *J. Geophys. Res.*, *88*, 5925–5938.

van Leeuwen, S. M., N. Dodd, D. Calvete, and A. Falqués (2006), Physics of nearshore bed pattern formation under regular or random waves, *J. Geophys. Res.*, *111*, F01023, doi:10.1029/2005JF000360.

Yu, J. (2006), On the instability leading to rip currents due to wave-current interaction, *J. Fluid Mech.*, *549*, 403–428.

Yu, J., and D. N. Slinn (2003), Effects of wave-current interaction on rip currents, *J. Geophys. Res.*, *108*(C3), 3088, doi:10.1029/2001JC001105.

N. Dodd, Environmental Fluid Mechanics Research Centre, Process and Environmental Division, Faculty of Engineering, University of Nottingham, University Park, NG7 2RD Nottingham, UK. (nick.dodd@nottingham.ac.uk)

R. Garnier, Applied Physics Department, Universitat Politecnica de Catalunya, Modul B4/5, c/o Jordi Girona, E-08034 Barcelona, Spain. (rgarnier@fa.upc.edu)

H. Hasan, Department of Mathematics and Basic Sciences, NED University of Engineering and Technology, University Road, Karachi 75270, Pakistan. (hhasan@neduet.edu.pk)